Letter

Elongation of Fe-Fe atomic pairs in the Invar alloy $Fe_{65}Ni_{35}$

N. Ishimatsu,[1,*] S. Iwasaki,[1] M. Kousa,[1] S. Kato,[1] N. Nakajima,[1] N. Kitamura,[2] N. Kawamura,[3] M. Mizumaki,[3] S. Kakizawa,[1] R. Nomura,[4] T. Irifune,[5] and H. Sumiya[6]

[1]*Graduate School of Advanced Science and Engineering, Hiroshima University 1-3-1 Kagamiyama, Higashihiroshima, Hiroshima 739-8526, Japan*

[2]*Department of Pure and Applied Chemistry, Faculty of Science and Technology, Tokyo University of Science, 2641 Yamazaki, Noda, Chiba 278-850, Japan*

[3]*Japan Synchrotron Radiation Research Institute (JASRI), SPring-8 1-1-1 Sayo, Hyogo 679-5198, Japan*

[4]*Hakubi Center/Graduate School of Human and Environmental Studies, Kyoto University, Sakyo, Kyoto 606-8501, Japan*

[5]*Geodynamics Research Center (GRC), Ehime University, Matsuyama 790-8577, Japan*

[6]*Advanced Materials R&D Laboratories, Sumitomo Electric Industries, 1-1-1 Itami, Hyogo 664-0016, Japan*

(Received 4 January 2021; revised 6 May 2021; accepted 28 May 2021; published 15 June 2021)

In this study, atomic-scale origin of the Invar effect, which is nearly-zero thermal expansion observed in the Invar alloy $Fe_{65}Ni_{35}$, was investigated by reverse Monte Carlo analysis using complementary data sets of extended x-ray absorption fine structure and x-ray diffraction. The interatomic distances of the nearest neighboring Fe-Fe atomic pairs were ∼0.02 Å longer than those of the Fe-Ni and Ni-Ni pairs at the minimum pressure in this study (0.6 GPa). The elongation in the Fe-Fe pairs was suppressed with increasing pressure, and the distances of the three pairs were comparable under pressures above the magnetic transition from ferromagnetic to paramagnetic phase at $P_c \approx 7$ GPa. Therefore, the Fe-Fe pairs dominantly contribute to the volume expansion due to the magnetovolume effect. Because a similar magnitude of elongation was observed in the Fe-Fe pairs of a non-Invar Fe-Ni alloy, we conclude that the Invar effect originates from the delicate balance between the number of Fe-Fe pairs and their elongation depending on the magnetization.

DOI: 10.1103/PhysRevB.103.L220102

Face-centered-cubic (fcc) Fe-Ni alloys containing 35–36 at.% Ni are known as Invar alloys. These alloys are characterized by the Invar effect, which shows a nearly-zero thermal expansion coefficient ($\alpha = 1.19 \times 10^{-6}$ /K) within a wide temperature range up to the Curie temperature ($T_C \sim$ 505 K). After the discovery of the Invar effect by Guillaume in 1897 [1], the origin of this anomalous thermal elastic property has been interpreted as cancellation of the thermal expansion by the shrinkage due to the large magnetovolume effect with increasing temperature [2]. However, the atomic-scale origin of the large magnetovolume effect is not fully understood so far.

Since the zero-thermal expansion of the lattice is related to the shallow curvature of the interatomic potential [3], the Invar alloy typically exhibits anomalously soft elastic properties under high pressures [4,5]. X-ray diffraction (XRD) experiments conducted by Dubrovinsky *et al*. revealed that the Invar effect occurs at pressures above pronounced bumps of the compression curve, where the softening behavior is observed [6]. They succeeded in initiating pressure-induced zero thermal expansions of $Fe_{55}Ni_{45}$ and $Fe_{20}Ni_{80}$ "non-Invar" alloys by compressing them to the softening pressure ranges of negative pressure derivatives for the bulk modulus.

The shallow interatomic potential and elastic softening behavior have been interpreted theoretically as a 2γ-state model [7–9], which hypothesizes two distinct spin states below T_C: a high-spin (HS) configuration associated with a large volume and low-spin (LS) one with a small volume. More recent *ab initio* calculations [3] demonstrated that the noncollinear spin alignment of Fe moments develops with increasing pressure whereas Ni spin moments maintain linear spin alignments even under pressure, which also explains the elastic softening behavior in the Invar alloy. The element-dependent response of magnetic structure under pressure motivated us to experimentally determine the local structure around Fe and Ni atoms separately. Several indications of the strong magnetovolume effect working on the Fe atoms have been found [10–15]. The relationship between the Fe-Fe interatomic distances and magneto-volume anomalies was investigated in crystalline intermetallic compounds [16,17]; however, direct observation of the elongated Fe-Fe interatomic distances is still a challenge because of the difficulties in distinguishing constituent elements in disordered alloys.

This Letter focuses on the atomic-scale origin of the magnetovolume effects in the Invar alloy. The atomic arrangement in a model structure composed of 4000 Fe/Ni atoms was investigated by reverse Monte Carlo (RMC) algorithm [18–21] combined with complementary data sets of extended x-ray absorption fine structure (EXAFS) and XRD under high pressure. The combination of three techniques allows element-specific local structural analysis of the atomic cluster, which also ensures long-range order in the model structure based on the fcc symmetry. This study revealed

*ishimatsunaoki@hiroshima-u.ac.jp

the elongation of nearest-neighboring Fe-Fe bonds compared with the lengths of Fe-Ni and Ni-Ni bonds in the ferromagnetic phase. Therefore, the large magnetovolume effect is attributed to the elongation of Fe-Fe atomic pairs. Interestingly, the elongation is not a unique characteristic of the Invar alloy; we observed comparable elongation of the Fe-Fe pairs in a $Fe_{55}Ni_{45}$ non-Invar alloy as well.

Polycrystalline $Fe_{65}Ni_{35}$ Invar and $Fe_{55}Ni_{45}$ non-Invar alloys were grained from ingots and pelletized for the EXAFS and XRD measurements. $Fe_{55}Ni_{45}$ non-Invar alloy has a 7.5 times larger thermal expansion coefficient ($\alpha =\sim 9 \times 10^{-6}$ /K) [22] and approximately 1.4 times higher Curie temperature ($T_C =\sim 720$ K) than $Fe_{65}Ni_{35}$ Invar alloy. Therefore, the $Fe_{55}Ni_{45}$ alloy is a good reference as the alloy exhibiting normal thermal expansion. The pressure dependences of XRD and EXAFS were measured on beamline 39XU at SPring-8 [23] independently using a fresh (uncompressed) pellet. The applied pressure to the sample was monitored using the conventional ruby fluorescence method. Nano-polycrystalline diamond anvils were utilized for the EXAFS measurement to prevent Bragg diffraction from the anvil crystals [24–26]. Fluorinert 70 + 77 solution was used as a pressure transmitting medium. All the measurements were performed at room temperature.

It is difficult to distinguish the neighboring Fe and Ni atoms to the x-ray absorbing atoms by conventional EXAFS analysis because of the small difference between the backscattering amplitudes of Fe and Ni [27,28]. Thus, previous EXAFS studies could not separate the like (Fe-Fe or Ni-Ni) and unlike (Fe-Ni or Ni-Fe) atomic pairs in the same shell [11,13,14]. In contrast, the RMC method constructs an atomic cluster and finds the best model of the atomic cluster that matches the experimental EXAFS profiles at Fe and Ni edges as well as the XRD patterns by trial and error iterations. Consequently, the length of each atomic pair can be evaluated from the determined cluster. In this study, we used the RMCProfile software for the RMC algorithm [19–21] and constructed a cubic cluster containing 4000 Fe/Ni atoms ($10 \times 10 \times 10$ fcc unit cells). Details of the experimental procedures and RMC calculations are provided in the Supplemental Material [29].

The RMC fits provided good agreement between the experimental and calculated profiles of the absolute values of Fourier transformed (FT) profiles ($|\mathrm{FT}\,[k^2\chi(k)]|$) at both the Fe and Ni edges of the Invar and non-Invar alloys [Figs. 1(a) and 1(b)]. The height of each peak increases with increasing pressure, which is also reproduced by the RMC calculations within an R range up to 6.0 Å. The prominent peaks at ~2.2 Å correspond to the first shells, where total 12 atoms of Fe and Ni participate as the first nearest neighboring (1NN) bonds around the x-ray absorbing atom. The R range up to 6.0 Å gives information on the atomic arrangements of 1NN–5NN atoms in the fcc lattice.

Figure 1(c) shows the experimental and fitted XRD patterns of the Invar and non-Invar alloys. Because the detecting area of the flat panel was limited to 50×50 mm^2 in size, we used 111 and 200 Bragg reflections to evaluate the lattice constant of the samples. Consequently, the RMC calculations are constrained only by the profiles of these two reflections. Sharp Bragg peaks are successfully generated by the RMC calculations at the same 2θ position of the experimental profiles,

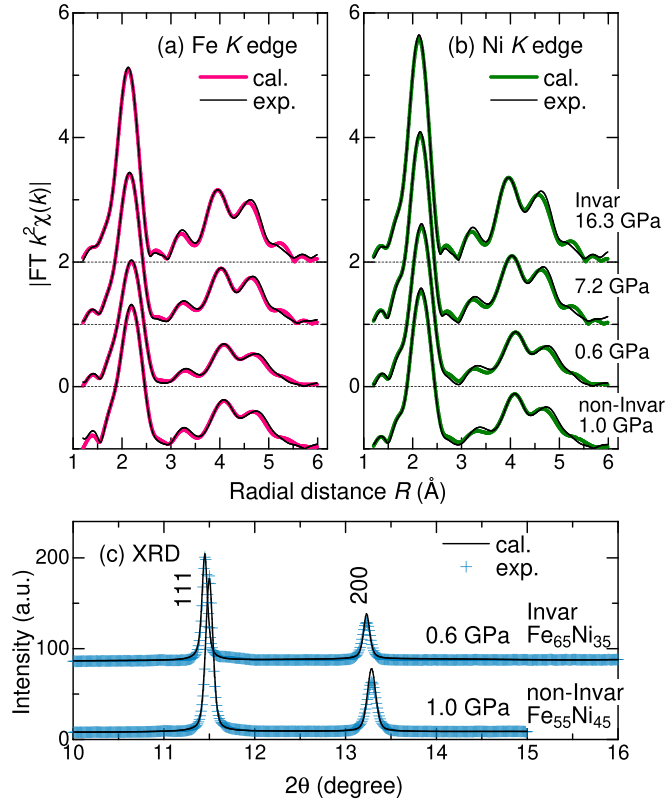

FIG. 1. Comparison of the experimental profiles with fits by the RMC calculations. Absolute values of Fourier transformed profiles ($|\mathrm{FT}\,[k^2\chi(k)]|$) of $Fe_{65}Ni_{35}$ Invar at (a) Fe K-edge and (b) Ni K-edges together with the data of non-Invar $Fe_{55}Ni_{45}$ alloy. (c) X-ray diffraction patterns under high pressures.

which ensures a long-range periodicity of the fcc symmetry in the atomic cluster as expected.

The partial pair distribution functions $g_{ij}(R)$ of Fe-Fe, Fe-Ni and Ni-Ni atomic pairs were determined from the atomic clusters optimized by the RMC calculations [30], where i and j represent Fe or Ni atoms. The $g_{ij}(R)$ profiles up to the 7NN pairs are plotted in Fig. 2(a). The vertical dashed lines represent the lengths of the atomic pairs expected from the lattice constant of a cluster with fcc symmetry. Small deviations in the peak positions from the fcc structure are observed in the first and second peaks. The maxima of the peaks appear at slightly lower positions with respect to the expected positions of the fcc lattice, while the deviation decreases with increasing R; peaks above 3NN are mostly located at the expected positions of the fcc lattice. As shown in Fig. 2(b), the determined atomic cluster conserves the sequential stacks of the (111) atomic planes, although much of the atoms are displaced from the ideal positions of the fcc lattice. Therefore, the RMC fits found a structure, in which the local structure was largely distorted; however, the disordered atomic cluster maintained the long-range periodicity to satisfy the Bragg law owning to the pseudo fcc symmetry.

A striking result of this study is the elongation of 1NN Fe-Fe pairs in comparison with 1NN Fe-Ni and Ni-Ni pairs. The enlarged plot of $g_{ij}(R)$ [see Fig. 3(a)] shows that the profile of 1NN Fe-Fe pairs has a peak at a longer R position than the

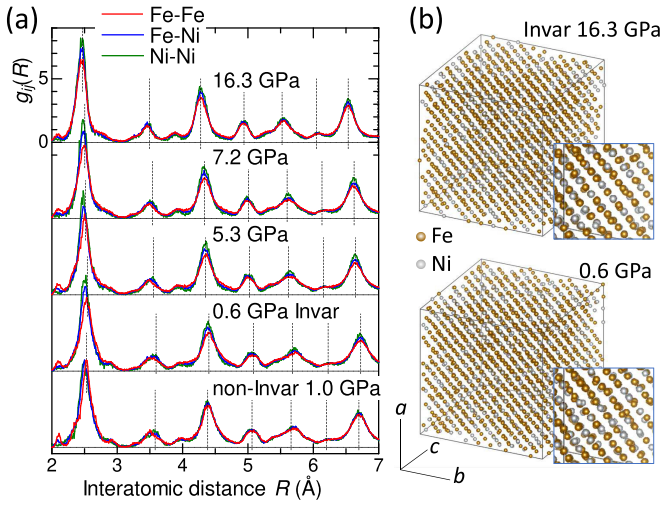

FIG. 2. (a) Partial pair distribution functions $g_{ij}(R)$ of i and j atomic pairs, where $i, j =$ Fe or Ni, in $Fe_{65}Ni_{35}$ Invar alloy at selected pressures together with the data of $Fe_{55}Ni_{45}$ non-Invar alloy. Each $g_{ij}(R)$ profile is normalized to approach to unity with increasing R. The vertical dashed lines indicate the lengths expected from the lattice constant of fcc structure. (b) Atomic clusters of the Invar alloy obtained by the RMC method. The clusters viewed from the $[11\bar{2}]$ direction are depicted. The insets display enlarged illustrations of the atomic cluster.

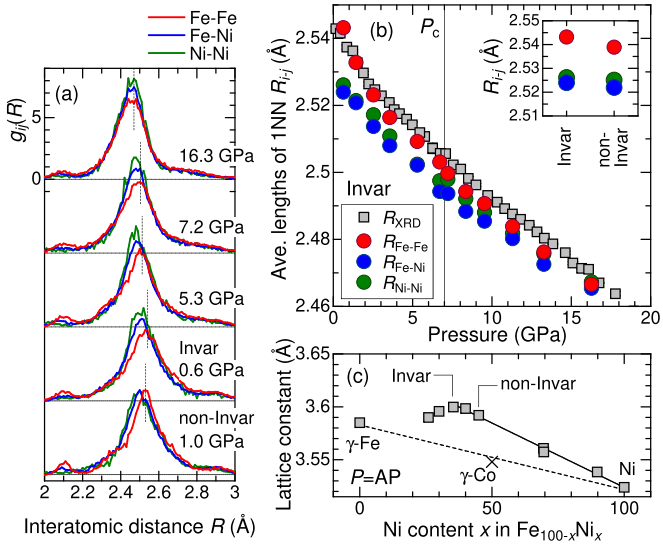

FIG. 3. (a) Enlarged plots of pair distribution functions $g_{ij}(R)$ ($i, j =$ Fe or Ni) of 1NN Fe-Fe and Fe-Ni and Ni-Ni atomic pairs in $Fe_{65}Ni_{35}$ Invar alloy and $Fe_{55}Ni_{45}$ non-Invar alloy. The vertical dashed lines indicate the lengths of 1NN pairs expected from the lattice constant of fcc structure. (b) Pressure dependences of the average length within a range of 0.6 Å centered on the 1NN peaks of Fe-Fe, Fe-Ni, and Ni-Ni pairs for $Fe_{65}Ni_{35}$ Invar alloy. The inset shows comparison of the average length of 1NN atomic pairs between $Fe_{55}Ni_{45}$ non-Invar alloy and $Fe_{65}Ni_{35}$ Invar alloy determined at the lowest pressures. (c) Ni composition dependence of the lattice constant of Fe-Ni alloys at ambient pressure. For comparison, lattice constants of antiferromagnetic γ(fcc)-Fe and ferromagnetic γ-Co are plotted [31].

profiles of Fe-Ni and Ni-Ni pairs at 0.6 GPa. The same trend is observed at 1.0 GPa for the $Fe_{55}Ni_{45}$ non-Invar alloy. As the pressure increases, the difference in $g_{ij}(R)$ profiles decreases gradually; the profiles of these three pairs exhibit peaks at approximately the same position of $R \approx 2.455$ Å at 16.3 GPa. To highlight the elongation of Fe-Fe atomic pairs, the average lengths of the 1NN atomic pairs, $R_{\text{Fe-Fe}}$, $R_{\text{Fe-Ni}}$, and $R_{\text{Ni-Ni}}$ were quantitatively determined. Considering the asymmetric profile around the 1NN peak, we utilized a numerical method to evaluate expected values of the profile as the average length. A range of 0.6 Å centered on the 1NN peak was used for the evaluation to cover the entire profile of the peak. Details of the numerical procedure are provided in the Supplemental Material [29]. The numerical averages are plotted as a function of pressure in Fig. 3(b). Compared with $R_{\text{Fe-Ni}}$ and $R_{\text{Ni-Ni}}$, the expansion of $R_{\text{Fe-Fe}}$ is of the size of 0.02 Å at the lowest pressure of the Invar alloy (0.6 GPa), which is slightly longer than the theoretically evaluated differences between Fe-Fe, Fe-Ni, and Ni-Ni atomic pairs [11]. Because the Fe-Fe pairs are more compressive than others, the elongation of $R_{\text{Fe-Fe}}$ decreases rapidly with increasing pressure; the evaluated $R_{\text{Fe-Fe}}$ reaches the values of $R_{\text{Fe-Ni}}$ and $R_{\text{Ni-Ni}}$ at pressures above 10 GPa.

The Invar alloy undergoes a pressure-induced magnetic transition from ferromagnetic phase to paramagnetic phase. The transition pressure of $P_c \sim 7$ GPa was determined by our previous measurements [10] of x-ray magnetic circular dichroism (XMCD) using the same batch of the Invar alloy sample (see the Supplemental Material [29]). We noted that the different values of P_c have been reported [32–36], however, all the reports observed steep suppression or collapse of the ferromagnetic order in $Fe_{65}Ni_{35}$ Invar alloy at pressures near the P_c value determined in this study. According to recent magnetization measurements, the magnetization disappears near 7 GPa at room temperature [34], whereas investigations of XMCD and x-ray emission spectroscopy conducted by two French groups reported magnetic transitions at higher pressures around 15 GPa [35,36]. They observed magnetic transitions to a nonmagnetic state at ~15 GPa followed by intermediate drops initiated by the transitions from an HS state to an LS state at pressures around 5 GPa.

The elongation and subsequent shrinkage of Fe-Fe pairs accompanied by the magnetic transition demonstrate that the volume changes due to the magnetovolume effect originate mainly from the Fe-Fe pairs, while the lengths of Fe-Ni and Ni-Ni pairs seem to contribute less to that. The volume expansion by the magnetovolume effect occurs to stabilize the ferromagnetic state by reducing the overlap between the electronic wave functions of $3d$ orbitals; therefore, the magnetovolume effect varies proportionally to the square of the magnetization [37]. Because the magnetization of the Invar alloy comprises the large magnetic moments of Fe atoms ($\sim 2.5\mu_B$) and small moments of Ni atoms ($\sim 0.6\mu_B$) [38,39], the large Fe moment is probably responsible for the repulsive force working in the Fe-Fe pairs. If we recall that the large Fe and small Ni moments are preserved in a wide range of Ni compositions of $Fe_{100-x}Ni_x$ alloy ($35 \leqslant x < 100$) [38], the interatomic repulsion in the Fe-Fe atomic pairs can be recognized as a common phenomenon in Fe-Ni alloys with fcc symmetry. Consequently, a similar elongation is observed

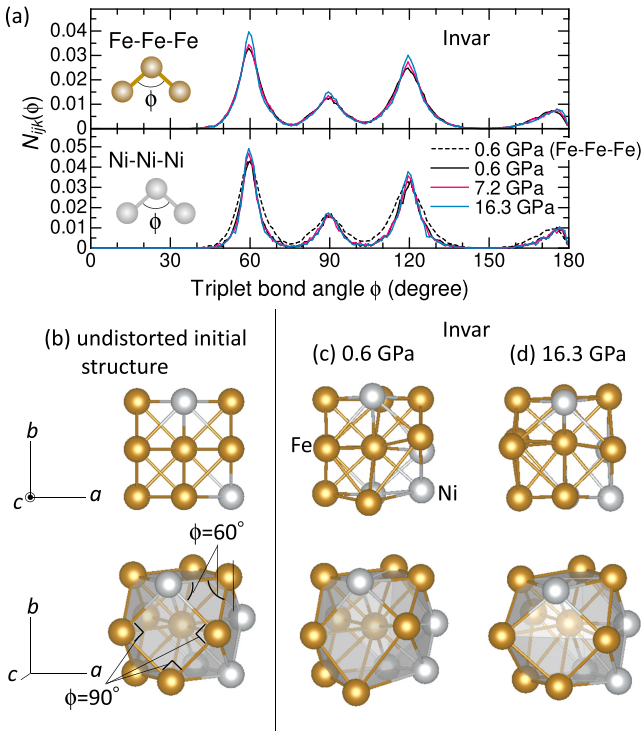

FIG. 4. Top: (a) angle distribution of Fe-Fe-Fe and Ni-Ni-Ni atomic triplets in the Invar alloy at selected pressures. Bottom: atomic clusters composed of 12 Fe/Ni nearest neighboring atoms and the central Fe atom at (b) initial undistorted model, (c) 0.6 GPa, and (d) 16.3 GPa. These clusters are picked up from the same position of the atomic cluster that we used for the RMC calculations.

in the Fe-Fe pairs of the $Fe_{55}Ni_{45}$ non-Invar alloy, as shown in the inset of Fig. 3(b).

In order to investigate the magnitude of the magnetovolume effect working in Fe-Ni alloys, we plot the lattice constants of Fe-Ni alloys at ambient pressure as a function of Ni composition x and demonstrate that the lattice constants are larger than those of antiferromagnetic γ(fcc)-Fe [31] and ferromagnetic γ-Co in the entire Ni composition range [see Fig. 3(c)]. The larger lattice constants reveal that the magnetovolume effect exists in Fe-Ni alloys to stabilize the ferromagnetic states, and the magnitude reaches a maximum in the narrow range of Ni composition covering the Invar alloy. Therefore, the lattice constant does not obey the Vegard's law but shows a linear decrease with increasing Ni content above $x \sim 35$. It is clear that a decreasing number of the repulsive Fe-Fe pairs in the Ni-rich alloys weaken the magnetovolume effect, which consequently leads to a linear decrease in the lattice constant.

To visualize the distortion in the short-range structure due to the different bond lengths between the three types of atomic pairs, histograms of the ϕ angle distributions, $N_{ijk}(\phi)$, are plotted in Fig. 4(a), where ϕ represents the angle of triplet atomic bonds composed of the adjacent i, j, and k atoms (i, j, k = Fe or Ni). In the undistorted fcc lattice, Fe/Ni atoms are surrounded by the 12 nearest neighboring Fe/Ni atoms, and these atoms form a polyhedron composed of regular triangles and squares of the atomic network, as illustrated in Fig. 4(b). Thus, $N_{ijk}(\phi)$ of the undistorted triplet atomic bonds shows a discrete angle distribution of $\phi = 60°$, $90°$, $120°$, or $180°$. In contrast, the actual $N_{ijk}(\phi)$ profiles are broadened around these angles due to the large distortion. Typical deformation in an atomic polyhedral is depicted in Figs. 4(c) and 4(d).

The Fe-Fe-Fe triplet bonds exhibit a border profile of $N_{ijk}(\phi)$ than the Ni-Ni-Ni bonds. $N_{ijk}(\phi)$ profile of the Fe-Fe-Fe triplet bonds is normalized and plotted by a dashed line in the bottom plot of Fig. 4(a) for comparison with the $N_{ijk}(\phi)$ profiles of Ni-Ni-Ni triplet bonds. Similar trends were observed for different types of triplet bonds, for example Fe-Fe-Ni and Ni-Fe-Ni, as shown in the Supplemental Material [29]. The triplet bonds composed of the larger number of Fe gave broader $N_{ijk}(\phi)$ distributions, implying that the elongated Fe-Fe pairs introduce the severe distortion to the atomic arrangement. The distortion probably occurs as a result of the stabilization of the ferromagnetic state by reducing the overlap between the Fe $3d$ orbitals. All $N_{ijk}(\phi)$ distributions become sharper with increasing pressure [29]. Therefore, the atomic arrangement approaches the undistorted polyhedron at higher pressures. However, we note that larger distortion remains in the local structure around Fe atoms compared with the structure around Ni atoms even at 16.3 GPa.

In summary, RMC analysis of the Invar alloy revealed the elongation of $R_{\text{Fe-Fe}}$ in comparison with $R_{\text{Fe-Ni}}$ and $R_{\text{Ni-Ni}}$ in the distorted atomic cluster with fcc symmetry. The elongation was suppressed with increasing pressure and disappeared, accompanied by the collapse of the ferromagnetic state at pressures above P_c. Therefore, the magnetovolume effect of the Invar alloy originates from the elongation of Fe-Fe atomic pairs. Interestingly, the elongation of Fe-Fe pairs occurred also in the $Fe_{55}Ni_{45}$ non-Invar alloy, indicating that the existence of longer Fe-Fe pairs due to the magnetovolume effect is a common phenomenon in the Fe-Ni alloy with fcc symmetry. Because the $Fe_{55}Ni_{45}$ non-Invar alloy undergoes a pressure-induced Invar effect at ~7 GPa [6], we conclude that the delicate balance between the number of Fe-Fe pairs and their elongation depending on the magnetization plays a crucial role in initiating the Invar effect.

The authors express their gratitude to Prof. H. Maruyama for supplying high-quality samples of the Invar alloy. The studies presented herein were partially supported by a Grant-in-Aid for Scientific Research on Innovative Areas (Grant No. 15H05829), Grant-in-Aid for Transformative Research Areas (A) "Hyper-Ordered Structures Science" (Grant No. 20H05880), and KAKENHI (Grants No. 17K05518 and No. 21H0104300). The x-ray absorption measurements were performed at SPring-8 with the approval of PRC-JASRI (Grants No. 2017B1304, No. 2017B1974, No. 2018B1355, and No. 2019A1530).

[1] C. Guillaume and C. H. Seances, Acad. Sci. **125**, 235 (1897).

[2] M. Hayase, M. Shiga, and Y. Nakamura, J. Phys. Soc. Jpn. **34**, 925 (1973).

[3] M. van Schilfgaarde, I. Abrikosov, and B. Johansson, Nature (London) **400**, 46 (1999).

[4] G. Oomi and N. Mori, J. Phys. Soc. Jpn. **50**, 2917 (1981).

[5] F. Decremps and L. Nataf, Phys. Rev. Lett. **92**, 157204 (2004).

[6] L. Dubrovinsky, N. Dubrovinskaia, I. A. Abrikosov, M. Vennström, F. Westman, S. Carlson, M. van Schilfgaarde, and B. Johansson, Phys. Rev. Lett. **86**, 4851 (2001).

[7] R. J. Weiss, Proc. Phys. Soc. **82**, 281 (1963).

[8] E. Wassermann, J. Magn. Magn. Mater. **100**, 346 (1991).

[9] L. Nataf, F. Decremps, M. Gauthier, and B. Canny, Phys. Rev. B **74**, 184422 (2006).

[10] K. Matsumoto, H. Maruyama, N. Ishimatsu, N. Kawamura, M. Mizumaki, T. Irifune, and H. Sumiya, J. Phys. Soc. Jpn. **80**, 023709 (2011).

[11] T. Yokoyama and K. Eguchi, Phys. Rev. Lett. **107**, 065901 (2011).

[12] J. R. Stellhorn, Y. Ideguchi, S. Hosokawa, N. Happo, T. Matsushita, K. Yubuta, M. Suzuki, H. Ishii, Y.-F. Liao, K. Kimura, and K. Hayashi, Surf. Interface Anal. **50**, 790 (2018).

[13] M. Kousa, S. Iwasaki, N. Ishimatsu, N. Kawamura, R. Nomura, S. Kakizawa, M. Mizumaki, H. Sumiya, and T. Irifune, High Pressure Res. **40**, 130 (2020).

[14] P. Gorria, R. Boada, A. Fernandez-Martinez, G. Garbarino, R. I. Smith, J. Chaboy, J. I. G. Alonso, D. Martinez-Blanco, G. R. Castro, M. Mezouar, A. Hernando, and J. A. Blanco, Phys. Status Solidi (RRL) **3**, 115 (2009).

[15] P. Gorria, D. Martínez-Blanco, M. J. Pérez, J. A. Blanco, A. Hernando, M. A. Laguna-Marco, D. Haskel, N. Souza-Neto, R. I. Smith, W. G. Marshall, G. Garbarino, M. Mezouar, A. Fernández-Martínez, J. Chaboy, L. Fernandez Barquín, J. A. Rodriguez Castrillón, M. Moldovan, J. I. García Alonso, J. Zhang, A. Llobet *et al.*, Phys. Rev. B **80**, 064421 (2009).

[16] P. Gorria, P. Alvarez, J. S. Marcos, J. L. Sanchez Llamazares, M. J. Perez, and J. A. Blanco, Acta Mater. **57**, 1724 (2009).

[17] D. Givord and R. Lemaire, IEEE Trans. Magn. **10**, 109 (1974).

[18] R. L. McGreevy and L. Pusztai, Mol. Simulation **1**, 359 (1988).

[19] M. G. Tucker, D. A. Keen, M. T. Dove, A. L. Goodwin, and Q. Hui, J. Phys.: Condens. Matter **19**, 335218 (2007).

[20] V. Krayzman, I. Levin, and M. G. Tucker, J. Appl. Crystallogr. **41**, 705 (2008).

[21] I. Levin, V. Krayzman, and J. C. Woicik, Appl. Phys. Lett. **102**, 162906 (2013).

[22] C. Guillaume, Comptes Rendus Acad. Sci. Paris **170**, 1554 (1920).

[23] N. Kawamura, N. Ishimatsu, and H. Maruyama, J. Synchrotron Rad. **16**, 730 (2009).

[24] T. Irifune, A. Kurio, S. Sakamoto, T. Inoue, and H. Sumiya, Nature (London) **421**, 599 (2003).

[25] N. Ishimatsu, K. Matsumoto, H. Maruyama, N. Kawamura, M. Mizumaki, H. Sumiya, and T. Irifune, J. Synchrotron Rad. **19**, 768 (2012).

[26] N. Ishimatsu, N. Kawamura, M. Mizumaki, H. Maruyama, H. Sumiya, and T. Irifune, High Pressure Res. **36**, 381 (2016).

[27] B. Ravel and M. Newville, J. Synchrotron Rad. **12**, 537 (2005).

[28] G. Bunker, *Introduction to XAFS* (Cambridge University Press, Cambridge, 2010), p. 85.

[29] See Supplemental Material at http://link.aps.org/supplemental/10.1103/PhysRevB.103.L220102 for details of the experimental procedures, RMC calculations, and supporting experimental results.

[30] D. A. Keen, J. Appl. Crystallogr. **34**, 172 (2001).

[31] M. Acet, H. Zähres, E. F. Wassermann, and W. Pepperhoff, Phys. Rev. B **49**, 6012 (1994).

[32] M. Abd-Elmeguid and H. Micklitz, Physica B **161**, 17 (1990).

[33] M. Abd-Elmeguid, B. Schleede, and H. Micklitz, J. Magn. Magn. Mater. **72**, 253 (1988).

[34] J. Kamarád, M. Míšek, and Z. Arnold, High Pressure Res. **34**, 365 (2014).

[35] L. Nataf, F. Decremps, J. C. Chervin, O. Mathon, S. Pascarelli, J. Kamarád, F. Baudelet, A. Congeduti, and J. P. Itié, Phys. Rev. B **80**, 134404 (2009).

[36] J. P. Rueff, A. Shukla, A. Kaprolat, M. Krisch, M. Lorenzen, F. Sette, and R. Verbeni, Phys. Rev. B **63**, 132409 (2001).

[37] E. Wohlfarth, Physica B+C **91**, 305 (1977).

[38] C. G. Shull and M. K. Wilkinson, Phys. Rev. **97**, 304 (1955).

[39] M. Collins, R. Jones, and R. Lowde, J. Phys. Soc. Jpn. Suppl. **17-B3**, 19 (1962).